



Article

Ni-Pd/ γ -Al₂O₃ Catalysts in the Hydrogenation of Levulinic Acid and Hydroxymethylfurfural towards Value Added Chemicals

Emilia Soszka ¹, Marcin Jędrzejczyk ¹, Ireneusz Kocemba ¹, Nicolas Keller ²  and Agnieszka M. Ruppert ^{1,*} 

¹ Institute of General and Ecological Chemistry, Faculty of Chemistry, Lodz University of Technology, 90-924 Łódź, Poland; e.soszka1991@gmail.com (E.S.); marjedrzejczyk@gmail.com (M.J.); ireneusz.kocemba@p.lodz.pl (I.K.)

² Institut de Chimie et Procédés pour l'Énergie, l'Environnement et la Santé, CNRS/University of Strasbourg, 67087 Strasbourg, France; nkeller@unistra.fr

* Correspondence: agnieszka.ruppert@p.lodz.pl

Received: 10 August 2020; Accepted: 1 September 2020; Published: 7 September 2020

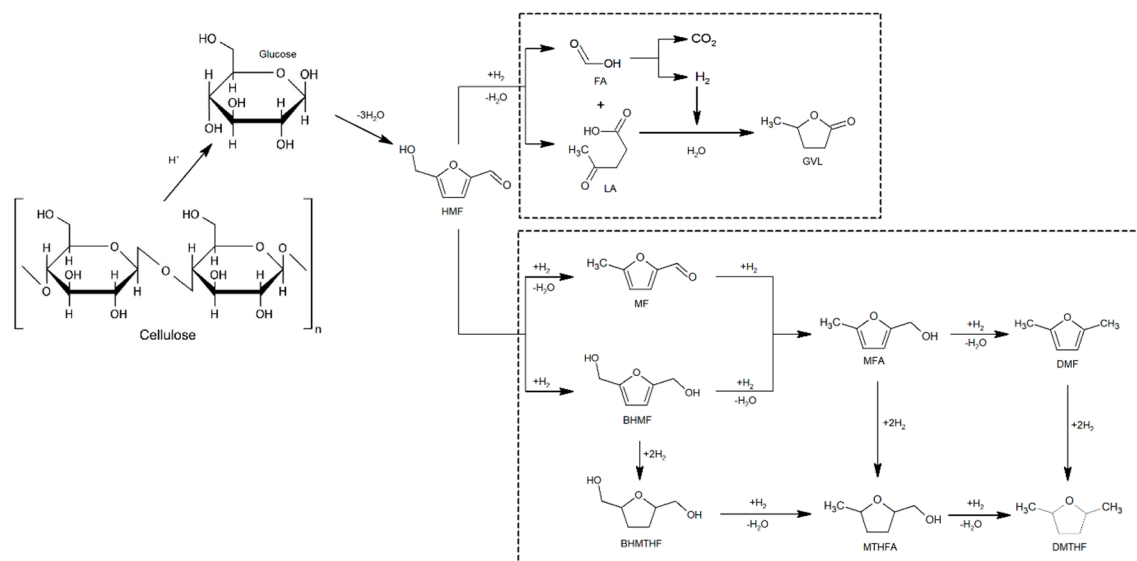


Abstract: γ -Al₂O₃ supported Ni-Pd catalysts with different Ni:Pd ratios were studied in the hydrogenation of two industrially-relevant platform molecules derived from biomass, namely levulinic acid and hydroxymethylfurfural. The bimetallic catalysts showed better performances in both processes in comparison to the monometallic counterparts, for which a too strong interaction with the alumina support reduced the activity. The behavior of the bimetallic catalysts was dependent on the Ni:Pd ratio, and interestingly also on the targeted hydrogenation reaction. The Pd-modified Ni-rich system behaves like pure Ni catalyst, but with a strongly boosted activity due to a higher number of Ni active sites available, Pd being considered as a spectator. This high activity was manifested in the levulinic acid hydrogenation with formic acid used as an internal hydrogen source. This behavior differs from the case of the Pd-rich system modified by Ni, which displayed a much higher Pd dispersion on the support compared to the monometallic Pd catalyst. The higher availability of the Pd active sites while maintaining a high surface acidity allows the catalyst to push the HMF hydrodeoxygenation reaction forward towards the green biopolymer precursor 2,5-bis(hydroxymethyl)-tetrahydrofuran, and in consequence to strongly modify the selectivity of the reaction. In that case, residual chlorine was proposed to play a significant role, while Ni was considered as a spectator.

Keywords: γ -Al₂O₃ supported Ni-Pd catalysts; selectivity; levulinic acid; γ -valerolactone; formic acid; hydroxymethylfurfural; 2,5-bis(hydroxymethyl)-tetrahydrofuran

1. Introduction

Biomass is considered as a very promising feedstock due to its abundance and availability. In particular, lignocellulosic waste materials have recently undergone extensive research in the field of renewable and sustainable resources for the industrial production of high-value chemicals and liquid fuels [1,2]. Two of the most promising intermediates (platform molecules) that can be derived from the hydrolysis of cellulose, and in particular from the dehydration of C-6 carbohydrates, are hydroxymethylfurfural (HMF), considered as an appealing starting material for various chemical synthesis owing to both its furan ring and the presence of two functional groups, as well as levulinic acid (LA). Their further hydrogenation enables the synthesis of high value-added molecules (Scheme 1, also indicating the notations used here).



Scheme 1. Reaction pathways of the HMF hydrodeoxygenation with the possible formed products and of the LA hydrogenation into γ -valerolactone (GVL) with formic acid (FA) as an internal hydrogen source, in the context of the global valorization of cellulose through initial hydrolytic hydrogenation.

The production of LA is favored using water as a solvent, and its further hydrogenation with subsequent cyclization gives γ -valerolactone (GVL) which can be used as a fuel additive, solvent, liquid fuel, and as a precursor of valuable chemicals [3,4]. The reaction can be performed using an internal hydrogen source, i.e., formic acid (FA) obtained in equimolar ratio with LA upstream of the process, for increasing the sustainability of the overall cellulose valorization process. By contrast, HMF production is favored in organic solvents, and its hydrogenation products are strongly dependent on both the catalysts and the reaction conditions [5]. Under appropriate conditions, HMF can be converted into 2,5-bis(hydroxymethyl)-tetrahydrofuran (BHMTHF), considered as an analogue of 1,3/1,4-cyklohexanedimethanol used for polyester production, through the total hydrogenation of the HMF furan ring, but taking into account that the aldehyde group needs to be saturated without further hydrogenolysis to 5-methyltetrahydrofurfuryl alcohol (MTHFA) or further to 2,5-dimethyltetrahydrofuran (DMTHF) [6]. BHMTHF can have several applications, as green solvent as well as pharmaceutical or nylon-6 polyamine intermediate [7–9].

Although Pd, Ru, Pt noble metal-based catalysts are most commonly used for both LA hydrogenation and HMF hydrodeoxygenation reactions [10,11], the tendency of using cheap, robust, non-noble based metals as supported catalysts is strongly manifested in the recent years [12,13]. Good performance for the selective hydrogenation of LA and HMF has been achieved with Ni-based catalysts.

Duarte et al. [14] showed that both Ni and Pd catalysts supported on γ -Al₂O₃ were active and selective towards the HMF decarbonylation in the aqueous phase at a hydrogen pressure of 4 bar and in the 137–189 °C range. Kong et al. [15] evidenced the difficulty of hydrogenating the C=C conjugated bonds in HMF using Ni-Raney catalysts, so that high selectivity towards BHMTHF could be easily reached, with no further hydrogenation into BHMTHF. High reaction yields towards BHMTHF were only possible with a prolonged reaction time (30 h) and a temperature of 100 °C. Further, Lima et al. [7] reported that Raney Ni in water was favoring 2,5-bihydroxymethylfuran (BHMF), with high selectivity of 60%, rather than BHMTHF (13% after 8 h of testing at 90 °C under 90 bar of hydrogen). They consequently proposed a two-step process combining first a Raney Cu to selectively form BHMF, further converted selectively to BHMTHF on Raney Ni (98%). The furan ring hydrogenation on monometallic Ni-based catalysts is therefore not preferential and requires severe reaction conditions and a high Ni content.

Regarding the LA hydrogenation, the approach of using FA as an internal hydrogen source provides an additional challenge to the reaction, as a selective FA decomposition is strongly required not only for reaching a high hydrogen yield but also for preventing from the surface poisoning by CO. Additionally, Ni can be also poisoned by hydrogen due to its strong adsorption on the surface [16]. Monometallic Ni catalyst can be, however, modified by the addition of a second metal, that can result in the formation of new active sites and can increase the catalyst stability due to the establishment of intermetallic interactions and the modification of Ni interaction with the support. In particular, Ni-Pd catalysts showed higher activity and selectivity as compared to their single counterparts in the hydrogenation of both HMF [17] and LA substrates [18]. Mihet et al. [19,20] showed that the introduction of small amounts (0.5%) of Pd and Rh noble metals to the 10% Ni/Al₂O₃ catalyst reduces the crystallite size, with higher activity following in both NO reduction and CO₂ methanation. It was also proposed that adding Pd to Ni facilitates its reduction and led to Ni-Pd systems with improved activity in the autothermal reforming of methane [21]. Another reason for the increased activity of Ni-Pd systems is the formation of the alloy. Regardless of the Ni:Pd ratio, Bayat et al. [22] proposed that the Ni-Pd alloy formation was responsible for the increase in the catalyst lifetime by reducing the carbon deposit formation during the methane decomposition reaction. The highest activity was observed for a 50:15 Ni:Pd ratio, while a too high content of Pd dopant led to decreased activity, due to the decrease in the catalyst surface area and to the particle agglomeration. Also, Zhang et al. [23,24] observed that adding Pd reduced both the sintering of Ni and the formation of the carbon deposit, with consequently increased stability of the catalyst in the hydrogen production from partial oxidation and steam reforming of n-octane.

There are, therefore, promising examples in the literature concerning the Ni-Pd systems, and the variety of composition, morphology, and consequently synthesis methods depend strongly on the targeted process. It is therefore difficult to predict which factors are crucial in the hydrogenation of the biomass-derived molecules. There is just proof of the principle examples evidencing the great potential of Pd-Ni systems in the hydrogenation of LA and HMF. Nakagawa et al. [17] reported that SiO₂ supported bimetallic Ni-Pd catalysts can be more active than Raney Ni and more selective than Pd/C for the HMF hydrogenation. Total hydrogenation of unsaturated compounds like HMF and furfural was achieved over the bimetallic Ni-Pd/SiO₂ catalyst, and the key role played by the alloy was hypothesized. When it comes to LA hydrogenation with FA as a hydrogen source reaction, we demonstrated recently that among the noble metal dopants (Pt, Pd, Ru, Rh) of Ni catalyst, Pd was the most active, and preliminary results showed that the activity of the bimetallic Ni-Pd catalysts could be tuned depending on the preparation method [18].

Therefore, a series of Ni-Pd bimetallic catalysts with different Ni:Pd ratios has been further developed for evaluation in both the HMF hydrogenation with external hydrogen source and the LA hydrogenation with FA as an internal hydrogen source. We focused on alumina supported catalysts since high isoelectric point supports such as γ -Al₂O₃ promote the HMF ring hydrogenation for forming BHMTFH [25], whereas supports showing Brønsted acidity, such as SiO₂, promote the formation of polyols and polymers by ring-opening [26]. The key factors having a role in the hydrogenation of both bioderived chemical substrates on Ni-Pd/ γ -Al₂O₃ catalysts are discussed, together with their impact on the catalyst behavior, notably in terms of activity and of reaction selectivity.

2. Results

2.1. Catalyst Characterization

The X-ray diffraction (XRD) patterns of mono and bimetallic catalysts are shown in Figure S1 with their corresponding description. In addition to the diffraction peaks corresponding to the γ -Al₂O₃ support, only broad peaks/shoulders revealed the presence of metallic Ni for the 4% Ni catalyst; they were further attenuated upon the addition of 1% Pd in the bimetallic 4%Ni-1%Pd sample, while not visible in the low Ni loading (1%) bimetallic counterpart sample. Further, no clear reflexes

corresponding to Pd were observed at ca. 40° for both monometallic Pd and bimetallic catalysts, independently of the Pd loading. This resulted from the low amount and small size of the crystallites, as well as from the low crystallinity of the alumina support.

The reduction profiles of mono and bimetallic catalysts (before the final reduction step) are shown in Figure 1. For monometallic nickel catalysts, a high-temperature hydrogen consumption peak starting at around 450 °C was observed. This may suggest the presence of NiO_x strongly interacting with the support or the formation of spinel [27,28]. In the case of the 1% Pd catalyst, a broad low-temperature reduction peak was noticed in the range of 50–200 °C. It may be related to the presence of small Pd particles having a strong interaction with the support [29]. Furthermore, it can be related to the reduction of PdO_xCl_y strongly interacting with the support [30]. It is worth noting that the reduction of bulk PdO is reported to take place at a lower temperature (55 °C) [31].

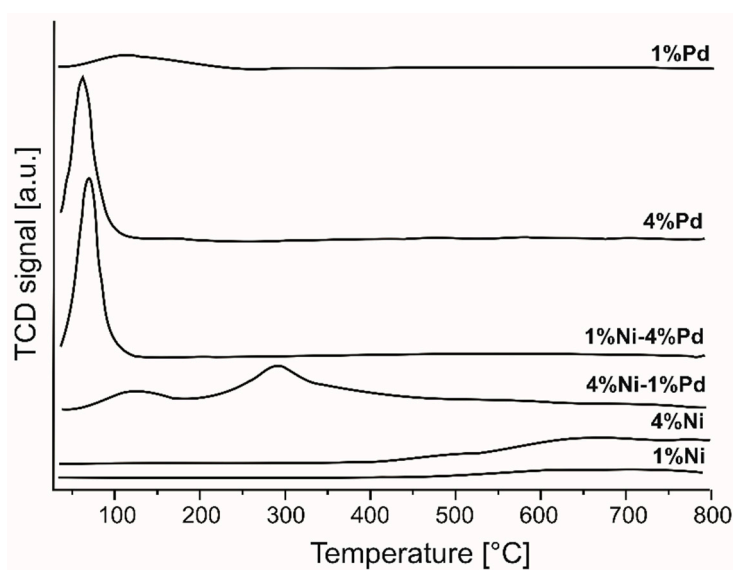


Figure 1. Temperature Programmed Reduction (TPR) profiles of mono and bimetallic catalysts after the oxidation step.

The increase in the Pd content from 1% to 4% allows us to observe a clear and sharp reduction peak with a maximum at 65 °C. This peak can be ascribed to the reduction of a mix of PdO and PdO_xCl_y species; therefore, it is possible that the Pd is interacting less with the support so that its reduction is facilitated [32].

The bimetallic Ni-Pd/ γ -Al₂O₃ catalyst reduction profiles are more complex than those of the monometallic catalysts. The shape of the reduction profiles is highly dependent on the Ni-Pd ratio. In all cases, we observe a low-temperature hydrogen consumption peak within the 30–140 °C range, associated with the reduction of Pd species. As the palladium content decreases, the low-temperature hydrogen consumption peak shifts towards a higher temperature, which may be related to the change of Pd crystallite size and in the interaction between the metals and the support. Large crystalline palladium is able to absorb hydrogen at room temperature within the metal structure, contrary to small well-dispersed palladium species [33]. To better illustrate those differences, the TPR profiles were recorded on the reduced samples (Figure S2). Only in the case of 4%Pd was a negative TPR peak observed, which was attributed to the decomposition of the Pd hydride (β -PdH₂) formed at room temperature from the absorption of atomic hydrogen within the structure of large size metallic Pd particles [31,34,35]. For the bimetallic samples, the absence of the hydride phase may indicate a good dispersion of palladium, staying in interaction with the second metal [34].

Furthermore, the presence of chlorine derived from the palladium precursor may facilitate the reduction of NiO_x and inhibit the formation of the interfacial NiAl_xO_y spinel [18]. For the 4%Ni-1%Pd catalyst, a high-temperature effect was observed in the temperature range 220–350 °C associated with

the reduction of NiO_x species [20,21,32], so that modifying the Ni catalyst with Pd as dopant facilitated the reduction of nickel. This effect could not be observed for the 1%Ni-4%Pd catalyst, due to the low nickel content. In addition, the low-temperature region reduction might also correspond to the reduction of a mix of NiO and PdO, as observed by Bayat et al. [22]. X-Ray Photoelectron Spectroscopy (XPS) and Time-of-Flight Secondary Ion Mass Spectrometry (ToF-SIMS) complementary analyses were performed for getting information about the catalyst surface and for identifying what kinds of surface species were present, as well as their effect on the interactions between the metal(s) and the support (Figure 2 and Table 1, respectively). In the case of the bimetallic 1%Ni-4%Pd catalyst, the Pd ion intensity (Pd⁻ and PdCl⁻) was higher than that recorded for the monometallic 4%Pd catalyst, which may suggest a better dispersion of palladium in the presence of a small amount of nickel, and thus may indicate that adding nickel improves the palladium dispersion in a Pd-rich catalyst [16,18]. It was worth noting that the surface of all Pd-containing catalysts contained residual chlorine species coming from the Pd precursor, and that were not completely eliminated during the thermal steps of the catalyst preparation. This was particularly pronounced on the 1%Ni-4%Pd bimetallic catalyst that contained a much higher amount of chlorine compared to that remaining in the corresponding 4%Pd monometallic counterpart, so that modifying the 4%Pd catalyst with 1%Ni unfavored the removal of the chlorine species during the thermal treatment, the highest amount of both PdCl⁻ and Cl⁻ ions being recorded on the Pd-rich bimetallic catalyst. However, the intensity of NiCl₂⁻ ions was similar for both bimetallic catalysts. By contrast, in the case of the Ni-rich catalyst, i.e., when Pd is only present as dopant, no difference in terms of chlorine ions intensity was observed compared to the monometallic Pd counterpart. Although the intensity of Ni ions was similar to that observed for the monometallic catalyst, the presence of additional NiCl₂⁻ ions suggested that Ni is also partially interacting with Cl species. The lower intensity of Pd, in this case, can suggest that Pd is partially covered by Ni species or that Pd is present as larger crystallites compared to the monometallic Pd counterpart.

Table 1. Normalized intensity of selected ions identified on the surface of the catalysts.

Catalysts	Cl ⁻ × 10 ⁻²	Ni ⁻ × 10 ⁻⁴	Pd ⁻ × 10 ⁻⁵	PdCl ⁻ × 10 ⁻⁴	NiCl ₂ ⁻ × 10 ⁻⁴
1%Ni	-	1.53	-	-	-
4%Ni	-	2.61	-	-	-
1%Pd	3.23	-	3.16	5.25	-
4%Pd	2.09	-	4.37	3.74	-
4%Ni-1%Pd	3.48	2.55	1.96	2.30	2.50
1%Ni-4%Pd	5.02	1.10	14.6	10.8	2.30

Figure 2 shows the palladium Pd 3p region, the Ni 2p_{3/2} region, and the Cl 2p region of XPS spectra recorded on the catalysts, while the wide scan survey spectra are reported as Figure S3. In general, the Ni 2p_{3/2} orbital spectra exhibit a complex feature with a broad multi-contribution envelope containing the core level peaks and shake-up satellite peaks corresponding to a multi-electron excitation and being characteristic of Ni species in oxidized states [36–38]. Except for the bimetallic 1%Ni-4%Pd catalyst, both metallic and oxidized states of Ni co-exist in all catalysts, with the broad and complex envelop showing a contribution at 855.7 eV corresponding to Ni in oxidized states that can be associated to Ni strongly interacting with the alumina support (aluminate) and/or to surface oxidized Ni, and another one at ca. 851.7 eV assigned to metallic Ni [39,40]. The 4%Ni monometallic sample was suggested to be more prone to surface oxidation than the catalyst with a lower loading, as evidenced by the highest intensity of the oxidized nickel contribution vs. the metallic one. By contrast, it is worth noting that no metallic nickel was observed at the surface of the bimetallic 1%Ni-4%Pd catalyst. Ni as a dopant of the Pd catalyst was only present as oxidized species, indicating that the reduction of the nickel at the surface is hindered in the Ni-modified Pd-rich catalyst.

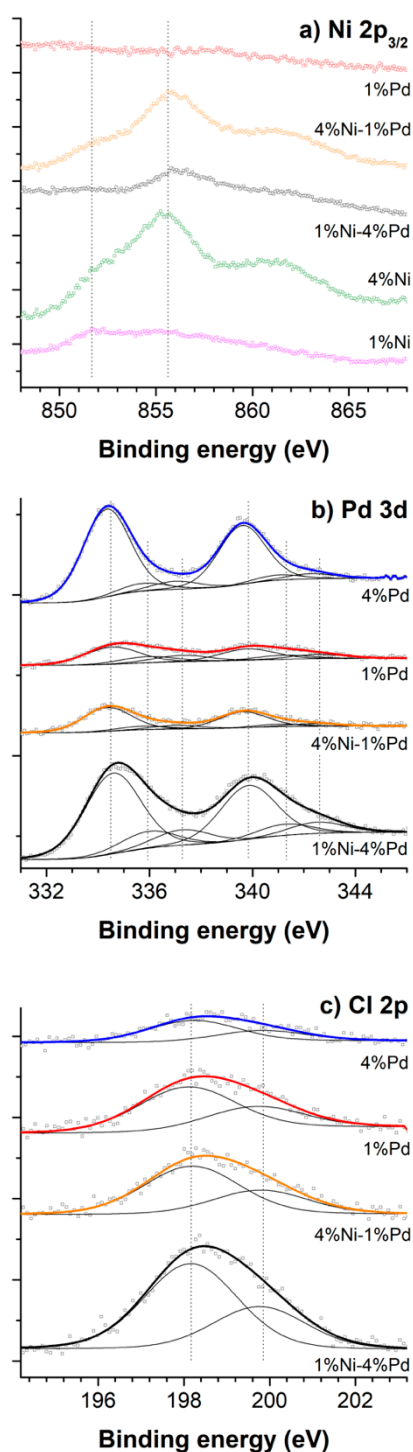


Figure 2. (a) Ni2p_{3/2}, (b) Pd3d, (c) Cl2p orbital XPS spectra of the mono and bimetallic catalysts.

Whatever the catalyst, the Pd 3d orbital spectra consist of three doublet contributions at 334.5 eV, 335.9 eV, and 337.2 eV (± 0.1 eV), each of them with a 3d_{5/2}-3d_{3/2} spin-orbit splitting constant of 5.26 eV. The two lower energy contributions were assigned to metallic and oxidized Pd surface species, respectively, with binding energy values being about 0.5 eV to 1.0 eV lower than those reported for bulk palladium, evidencing metal-support interaction between Pd and with Al₂O₃. The data do not allow us to distinguish whether oxidized surface Pd corresponds to Pd oxide(s) or hydroxide(s). The higher energy doublet contribution might be assigned to Pd atoms in interaction with residual chloride species (e.g., as oxychloride species, as already suggested for chloride precursor-derived metallic catalysts

such as Pd/Al₂O₃, Ru/C or Ru/Al₂O₃ [41–43]). Indeed, the presence of residual chlorine species at the surface of all the Pd-based catalysts was evidenced on the survey spectra, while the Cl 2p orbital spectra showed the usual 2p_{3/2}–Cl 2p_{1/2} doublet contribution at 198.2–199.8 eV with a spin–orbit splitting constant of 1.6 eV. This confirmed that the chlorine species were not completely eliminated during the thermal oxidation and reduction pretreatment steps [44–46], in agreement with ToF-SIMS results.

In line with the ToF-SIMS results, it was noted that modifying the 4%Pd catalyst with Ni improved the Pd dispersion at the alumina surface, with an increase in the Pd/Al surface atomic ratio from 0.019 to 0.024. Further, the presence of Ni was detrimental to the elimination of the chlorine species from the catalyst surface, with a strong increase of the Cl surface atomic percentage from 0.33% for the monometallic 4%Pd catalyst to 1.34% for the Ni-modified Pd-rich catalyst. This was as well evidenced by the simultaneous increase of both Cl/Al and Cl/Pd surface atomic ratios from 0.01 and 0.53, respectively, to 0.04 and 1.70 when modifying the 4%Pd catalyst with 1% of Ni.

Fourier Transform Infrared spectra (FTIR) spectra of CO adsorbed on the monometallic and bimetallic catalysts recorded under pressure are shown in Figure 3a,b, respectively. The spectra of nickel catalysts obtained under pressure showed only the band at 2056 cm⁻¹ attributed to CO linearly adsorbed on Ni⁰ or physically adsorbed on nickel as the tetracarbonyl Ni(CO)₄ band [47,48] being more intense in the spectrum of the 4% Ni catalyst. The strong decrease of the band intensity recorded after CO evacuation suggests the weak adsorption of CO on the nickel crystallites (Figure S4).

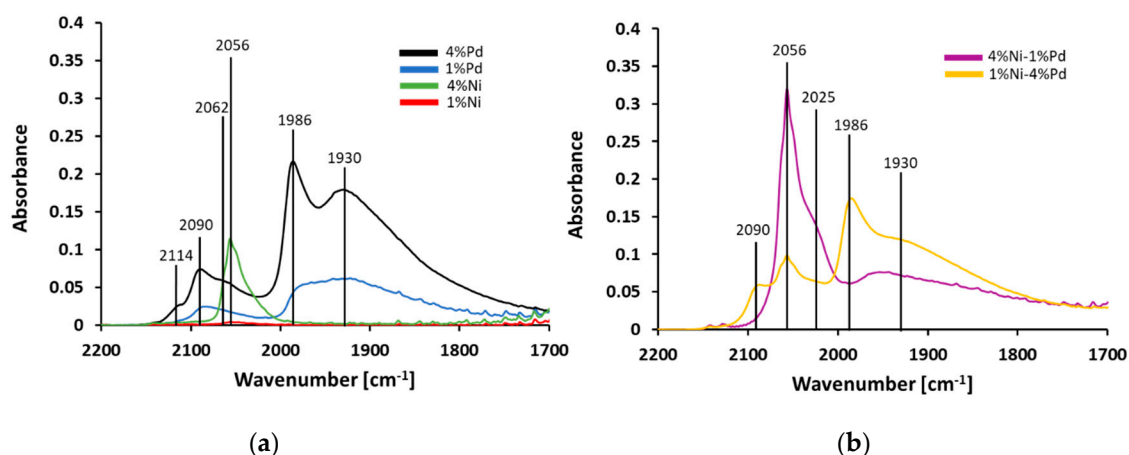


Figure 3. FTIR spectra of CO adsorbed on the surface of (a) the monometallic and (b) the bimetallic catalysts recorded under CO pressure.

In the spectra of palladium catalysts, clear bands are visible at 1930 cm⁻¹ and 1986 cm⁻¹, assigned respectively to the bridge-bonded CO at metal corner/edge sites and on metal (low-index plane) facets, as a result of the weaker dipole-dipole coupling on crystallite corners/edges. The band at 2090 cm⁻¹ was assigned to linear-bonded CO on metal atoms [49–51] and exhibited also two shoulders at 2062 cm⁻¹ and 2114 cm⁻¹. The shoulder at the lower wavenumber was reported to correspond to the linear CO adsorption on Pd crystallite planes with lower coordination in comparison to the band at 2090 cm⁻¹ [52], and that at the higher wavenumber of 2114 cm⁻¹ was indicated to characterize the linear adsorption of CO on highly dispersed cationic Pd^{δ+} [53].

Moreover, although on both monometallic Pd catalysts there is bridged CO adsorption on both facet and corner/edge sites, the adsorption is more intense on corner/edge sites for 1%Pd, and on facets for 4%Pd. This can be related to different sizes for the metal crystallites and with their different surface features being dominated by low index planes or corner/edge atoms [54].

All the spectra recorded for CO adsorption on bimetallic catalysts showed bands of bridge-bonded CO on palladium and of CO linearly adsorbed on nickel, regardless of the metal ratio used. However, the type of CO adsorption depends on the Ni:Pd ratio. Indeed, for the Pd-rich catalyst (ie., 1%Ni-4%Pd),

the band at 2090 cm^{-1} characteristic for the linear adsorption of CO on palladium crystallites is visible with similar intensity than for the monometallic counterpart.

However, only a limited bridged CO adsorption is observed on the Pd corners/edges, as evidenced by the decrease in the intensity of the band at 1930 cm^{-1} . This might result from the partial blockage of the palladium corners/edges by heteroatoms, namely nickel and/or chlorine atoms. By contrast, in the spectra of the Ni-rich catalyst (4%Ni-1%Pd), comparing the intensity of the band at 2056 cm^{-1} clearly revealed that the addition of Pd causes an increase in the number of Ni adsorption centers. This increase of adsorption can result from the weaker interaction of Ni with the support surface in comparison to the monometallic 4%Ni counterpart, in agreement with the TPR results. The higher number of metallic Ni centers available was also confirmed by the shoulder at 2025 cm^{-1} , characteristic of linear CO bounded to one nickel atom, and that is not observed for the monometallic nickel catalysts [55].

In addition, FTIR studies can be associated to CO chemisorption performed at ambient pressure (Table 2). As shown above, after pressure release, the CO adsorption on Ni crystallites is weak, unlike what is observed for Pd adsorption centers (Figure S4). Therefore Ni-rich catalysts showed lower CO chemisorption uptakes than the Pd-based catalysts; however, the chemisorption capacity was higher on the Ni-rich bimetallic catalyst (4%Ni-1%Pd) than on the monometallic Ni counterpart. The highest amount of chemisorbed CO was observed for the monometallic 4%Pd catalyst that showed the most intensive bands in FTIR spectra, followed by the Pd-rich bimetallic catalyst (1%Ni-4%Pd) for which the FTIR spectra also exhibited lower intensity bands in comparison to the 4%Pd monometallic catalyst. This can be related with the presence of chlorine (ToF-SIMS, XPS study) that can influence the chemisorption capacity, as well as with the possible blockade of Pd corners and edges, with consequently a lower CO chemisorption.

Table 2. CO chemisorption and NH_3 -TPD results of the Ni-Pd catalysts.

Catalysts	CO Uptake ($\mu\text{mol/g}$)	Acidity (mmol/g)
1%Ni	4	0.878
4%Ni	20	0.852
1%Pd	16	0.990
4%Pd	61	1.212
4%Ni-1%Pd	25	1.210
1%Ni-4%Pd	31	1.150
$\gamma\text{-Al}_2\text{O}_3$	-	0.980

The acidity of the catalysts was derived from the temperature-programmed desorption of NH_3 and expressed as the molar amount of NH_3 adsorbed per gram of catalyst (Table 2). It can be seen that the acidity of the monometallic Ni catalysts is lower than that of the support itself and is decreasing with the increase in the metal loading, which is related to the coverage of the acid sites of the support [56].

In contrast to the nickel catalysts, the acidity of Pd-based catalysts (mono and in particular bimetallic) either does not decrease or is even higher than that of bare $\gamma\text{-Al}_2\text{O}_3$. There are several factors that could be responsible for that phenomenon. Firstly, it can be related to the presence of residual chlorine derived from the palladium precursor (ToF-SIMS, XPS). Although chlorine is a Brønsted base, its electron-withdrawing properties may change the acid-base balance of the alumina supported palladium catalyst due to its interaction with metal and oxide. As a result of the interaction with the surface of the aluminum oxide, chlorine builds into its structure, replacing the basic centers and thereby strengthening the acid centers [57,58].

Secondly, the interaction between chlorine and palladium results in the electron-deficient character of the palladium metal [59–63], which can consequently enhance the NH_3 adsorption. What is more, metallic palladium and nickel are also considered as NH_3 adsorption sites, and this adsorption is facilitated in the case of bimetallic catalysts due to the decrease of the Ni/support interaction [64].

2.2. Catalytic Activity in the Hydrogenation of LA

The catalytic activity of the mono- and bi-metallic catalysts with different Ni-Pd ratios in the LA hydrogenation using FA as a hydrogen source is reported in Table 3 in terms of both FA and LA conversions and of yield to GVL. In general, both monometallic Pd catalysts exhibited higher activity in the levulinic acid hydrogenation with formic acid as an internal hydrogen source (FALA) than the monometallic nickel catalysts, for which only low FA decomposition (26%–31%) was observed with consequently a very low LA conversion (5%–6%) and no production of GVL, independently of the Ni metal loading. We showed that nearly full FA conversion is necessary for initiating the subsequent LA hydrogenation. This is related to the strong adsorption of the formate intermediate on the active metal sites that hinders the adsorption of LA [18,41]. Despite a full FA decomposition, the monometallic Pd catalysts exhibited a low LA hydrogenation level (14%–16%) regardless of the Pd content, with a very low GVL yield of about 8%–12%.

By contrast, both bimetallic Ni-Pd catalysts displayed significantly higher activity in the combined FALA reaction than the different monometallic counterpart catalysts independently of the Ni:Pd ratio. Whereas full FA decomposition was obtained in both cases, a significantly higher LA conversion and GVL yield of 43% and 37%, respectively, could be achieved on the bimetallic Ni-rich catalyst (4%Ni-1%Pd), while the highest activity was observed for the catalyst with the highest Pd content (1%Ni-4%Pd), which allowed us to obtain an LA conversion of 50% with a GVL yield of 47%.

Table 3. Activity of mono- and bimetallic Ni-Pd/ γ -Al₂O₃ catalysts in the simultaneous FA decomposition and LA hydrogenation into GVL, expressed in terms of both FA and LA conversions and of GVL yield.

Catalysts	Conversion (%)		Yield (%)
	FA	LA	GVL
1%Ni/ γ -Al ₂ O ₃	31	6	0
4%Ni/ γ -Al ₂ O ₃	26	5	0
1%Pd/ γ -Al ₂ O ₃	100	14	8
4%Pd/ γ -Al ₂ O ₃	100	16	12
4%Ni-1%Pd/ γ -Al ₂ O ₃	100	50	47
1%Ni-4%Pd/ γ -Al ₂ O ₃	100	43	37

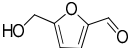
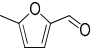

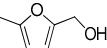
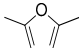
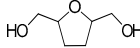
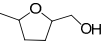
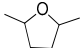
Reaction conditions: 190 °C; 2 h; 0.6 g of catalyst; 1 g LA and 0.4 mL FA corresponding to an equimolar LA:FA ratio; 30 mL water.

2.3. Catalytic Activity in the Hydrogenation of HMF

The conversion and the product yields in the hydrogenation of HMF obtained for the mono and bimetallic catalysts with different Ni-Pd ratios are shown in Table 4. In given reaction conditions, full conversion was obtained for most of the catalysts, with the exception of the monometallic Ni catalyst.

In the case of the monometallic Ni catalyst, the reaction is not selective, and the main products observed were BHMTFH and MTHFA, giving also the highest number of other by-products. The lack of DMF could suggest that the reaction proceeds via the carbonyl group hydrogenation, followed by the ring hydrogenation to form BHMTFH and further hydrogenolysis to MTHFA and DMTHF. Although for Ni catalysts the selectivity path depends strongly on both the catalyst properties and the reaction conditions, the above-proposed path is supported by the literature, particularly for alumina supported Ni catalysts [65], or for Raney Nickel in milder hydrogenation conditions [7]. According to the literature, the presence of a support with a high isoelectric point (like alumina) can additionally enhance the reduction of the aromatic ring [25].

Table 4. The activity of monometallic and bimetallic Ni-Pd/ γ -Al₂O₃ catalysts in the HMF hydrogenation, expressed in terms of HMF conversion and of the different product yields.

Catalysts	Conversion (%)				Product Yields (%)				
	HMF 	MF 	BHMF 	MFA 	DMF 	BHMTHF 	MTHFA 	DMTHF 	Others
4%Ni	90	2	0	0	0	34	27	3	24
4%Pd	100	1	0	1	32	57	3	6	0
4%Ni-1%Pd	100	1	1	0	0	47	0	50	0
1%Ni-4%Pd	99	1	0	1	18	76	0	3	0

Reaction conditions: 220 °C; 4 h; 0.3 g of catalyst; 1 g HMF, 30 mL 1,4-dioxane and 30 bar H₂.

In contrast, the monometallic 4%Pd shows a high yield of BHMTHF (57%), with the formation of a significant amount of DMF (32%). The formation of DMF can occur both via the hydrogenolysis of HMF to 5-MF, or via the hydrogenation its aldehyde group to form BHMF. However, while BHMF is the postulated intermediate in the literature for the DMF formation, BHMF can further be hydrogenated to BHMTHF. In our case, the subsequent hydrogenolysis of BHMTHF on Pd/Al₂O₃ is, however, suppressed, as only marginal yields to MTHFA and DMTHF were observed. It is known, however, that the hydrogenolysis of the side chains in HMF is competitive with the ring hydrogenation on Pd catalysts, so that is difficult to control this selectivity [66,67].

As far as the bimetallic catalysts are concerned, the above-described effects are amplified. The addition of 1%Ni to the 4%Pd catalyst promoted the formation of BHMTHF, so that the bimetallic 1%Ni-4%Pd catalyst strongly overcomes its 4%Pd monometallic counterpart with a high yield of BHMTHF of 76%. Interestingly, the selectivity of the Pd-rich catalyst is kept to the same product. Having in mind that the Pd-supported catalyst is quite selective towards BHMTHF, especially at high temperatures [14], this suggests that here, Pd is the active site, whereas the Ni dopant remains a spectator for the reaction. The higher activity of the bimetallic catalysts in comparison to the monometallic counterparts and Raney Nickel was also shown by the group of Tomishige for systems supported on silica, but they did not observe this behavior related with the selectivity on silica-supported materials [17].

Adding 1%Pd to the 4%Ni catalyst allowed the formation of equal amounts of BHMTHF and DMTHF, avoiding the formation of by-products, as in the case of monometallic Ni. Once again, a similar effect was observed for the Ni-rich bimetallic system. We observed typical behavior in this reaction for monometallic Ni, namely ring hydrogenation and BHMTHF formation and further hydrogenolysis via MTHFA to DMTHF. The difference was related to the fact that this reaction proceeds to a much higher extent, as much higher yields of BHMTHF and DMTHF were obtained with the suppression of byproducts. In this case, Ni was considered as an active site, similarly to what is described in the literature for Ni-Au systems, for which the role of Au was to alter the Ni properties, e.g., by preventing surface poisoning due to a beneficial change in the adsorption energy of reaction substrates.

3. Discussion

This work aimed at getting a deeper understanding of the influence of the modification of Pd and Ni catalysts by dopants on their physicochemical properties and their activity in two important bio-based processes. HMF hydrodeoxygenation and LA hydrogenation reactions were consequently chosen to illustrate selectivity and activity performance issues, respectively. Ni/ γ -Al₂O₃ shows poor activity in both processes due to the existence of very strong interactions between the nickel phase and the alumina support that are favoring the formation of the hardly reducible NiAl₂O₄ spinel interfacial phase [68], resulting in a reduction of the number of active metallic sites [69]. In contrast, they create new active centers that are reactive for the hydrogenation of the furan ring.

The modification of the Ni-rich catalysts with Pd significantly boosted the activity performance, with a twofold role played by the Pd dopant. This role is not only limited to the direct Pd influence, but also relates to the presence of residual chlorine derived from the Pd metallic precursor. Firstly, we observed a changed affinity of Ni with the alumina support that results from the interaction of Ni with Pd and chlorine [18]. Consequently, for Ni-rich bimetallic catalysts, this results in the higher availability of Ni-active sites.

Modifying the Ni catalyst with Pd lowered the catalyst reduction temperature, as evidenced by CO-adsorbed FTIR and CO chemisorption, in agreement with the literature [70]. Additionally, during the reaction in a reductive atmosphere, the reduction of Ni can be favored by a spillover effect taking place on the surface Pd, on which H₂ molecules dissociate into atomic hydrogen. The stronger reducing power of atomic hydrogen compared to molecular gaseous H₂ is consequently beneficial for the hydrogenation reactions, while it can also favor an easier reduction of surface NiO_x species after fast diffusion into the Ni crystal lattice [21,70].

We suggest that the dopant metal in a low content influences directly the surface properties of the Ni-Pd catalysts, so that it is somehow indirectly responsible for the change in the catalytic performances in both HMF hydrodeoxygenation and LA hydrogenation. The selectivity of the reactions was kept for the same product, while the catalyst activity was boosted compared to the monometallic counterparts.

The Pd-modified Ni-rich system, therefore, behaves like the pure Ni catalyst but with a strongly boosted activity, and the role of Pd can be considered as a spectator. This is especially visible in the HMF hydrodeoxygenation, and this stronger activity could be related to the higher number of Ni active sites. This higher number of active sites is also manifested in the FALA reaction, providing the highest activity is the reaction.

The situation is different in the case of the Ni-modified Pd-rich system, for which a higher dispersion of Pd was manifested compared to the monometallic Pd catalyst (ToF-SIMS, XPS study). A higher number of active sites, while preserving the very high acidity of the surface of the catalyst, help to push the HMF hydrodeoxygenation forward towards BHMTHF [10]. Pd generally favors the hydrogenation of the furan ring because of the strong interaction between the narrow d band of Pd and π bonds [5]. Additionally, the Pd-supported catalyst is quite selective towards BMHTHF, especially at high temperatures [14]. Higher activity of this bimetallic palladium-rich catalyst in comparison to the monometallic Pd counterpart could be also related to the limited formation of β -Pd hydrate, which could poison palladium. This suggests that here, Pd is the active site, whereas the Ni dopant remains a spectator for the reaction.

Furthermore, the very high content of chlorine of the catalyst (even largely higher than for the monometallic 4%Pd counterpart) has a significant effect. The higher electronegativity of Cl vs. Ni (with the high electron withdrawing-properties of Cl) can lead to an electronic depletion of the Ni species, which might explain the weaker resistance of Ni to surface oxidation, i.e., a hindering of the Ni reduction. A similar effect between neighboring Pd and Ni atoms can also be suggested due to the lower Ni electronegativity. By contrast, this Cl^- and Pd^- induced effect on the electronic state of the Ni species is not preponderant in the Ni-rich catalyst because of the significantly smaller amount of chlorine and Pd atoms compared to the dominant Ni.

4. Materials and Methods

4.1. Materials and Chemicals

$\text{Ni}(\text{NO}_3)_2 \cdot 6\text{H}_2\text{O}$ (100% pure, Chempur, Piekary Śląskie, Poland), PdCl_2 (98.5% pure, Chempur, Piekary Śląskie, Poland), Al_2O_3 (Fluka, type 507, Buchs, Switzerland), formic acid (85% purity, Chempur, Piekary Śląskie, Poland), levulinic acid (98% purity, Sigma Aldrich, Poznań, Poland), hydroxymethylfurfural (98% purity, FluoroChem, Hadfield, UK) and 1,4-dioxane (98% pure, POCH, Gliwice, Poland) were used as received.

4.2. Catalyst Preparation

$\gamma\text{-Al}_2\text{O}_3$ supported bimetallic Ni-Pd (5 wt.%) catalysts with different metal ratios (1:4 and 4:1) were prepared following the wet impregnation method using $\text{Ni}(\text{NO}_3)_2 \cdot 6\text{H}_2\text{O}$ and PdCl_2 as metal precursors in water. All catalysts were calcined at 500 °C for 5 h under a flow of air with a temperature ramp rate of 5 °C·min⁻¹ and further reduced under H_2 flow for 1 h at 650 °C (5 °C·min⁻¹). The monometallic counterpart catalysts were also prepared following a similar protocol with 1 wt.% and 4 wt.% of metals for comparison.

4.3. Characterization Techniques

Temperature-Programmed Reduction (TPR) was carried out on the AMI1 system (Altamira Instr., Pittsburgh, PA, USA) using a thermal conductivity detector for studying the catalyst reducibility. TPR was performed on the samples after the calcination step. TPR profiles were recorded with

a 10 °C/min heating rate, using a mixture of 5/95 vol./vol.% H₂/Ar at a space velocity of $3.1 \times 10^{-9} \text{ g}\cdot\text{s}^{-1}\cdot\text{cm}^{-3}$.

Fourier Transform Infrared spectra (FTIR) of the adsorbed CO were recorded on a Nicolet 6700 spectrometer equipped with a liquid nitrogen cooled MCT detector and a diffuse reflectance environmental chamber (Specac Ltd., Orpington, UK). The catalyst was placed in a sample holder, reduced in situ at 650 °C in flowing 5% H₂/Ar for 1 h, and cooled to room temperature under Ar flow before the recording of the background spectrum. Two types of CO-adsorbed FTIR spectra were collected, i.e., under the pressure of CO and at ambient pressure after its evacuation. The CO absorption spectra under a pressure of 5 bars of 5% CO/Ar were obtained after saturation of the sample surface for 30 min, while the spectra at ambient pressure were recorded after the release of the CO pressure. All spectra were collected at a resolution of 4 cm⁻¹ accumulating 64 scans.

CO chemisorption studies were carried out with the use of a PEAK-4 apparatus [71]. Also, 0.4 g of catalyst was placed in a glass tube reactor with an internal diameter of 5 mm and was in-situ reduced at the temperature of 650 °C for 1 h in H₂ stream with a flow rate of 40 cm³·min⁻¹. Then, the reactor was cooled to room temperature, and the flow of H₂ was replaced by Ar. Next, pulses of 0.05 cm³ CO were introduced to the reactor using a six-way valve, and an infrared gas analyzer (Fuji type ZRJ-4, Fuji Electric, Tokyo, Japan) was used for monitoring the changes in the CO concentration.

Temperature-Programmed Desorption (TPD) of NH₃ was performed for studying the catalyst acidity. The NH₃-TPD experiments were implemented in a home-made quartz-based flow micro-reactor. Before all experiments, the surface of the catalyst was cleaned under hydrogen flow for 30 min at 500 °C. The catalyst was then cooled down to 100 °C, and NH₃ was adsorbed on the surface of the catalyst for 15 min at 100 °C. Prior to measurement, physically adsorbed NH₃ was removed from the surface of the catalyst by He flow cleaning for 15 min before cooling down the sample to the ambient temperature. The NH₃-TPD experiment was performed from room temperature to 500 °C with a 25 °C/min heating ramp.

Time-of-Flight Secondary Ion Mass Spectrometry (ToF-SIMS) measurements were carried out in an ION-TOF GmbH instrument (TOF-SIMS IV, IONTOF GmbH, Münster, Germany) equipped with a 25 kV pulsed Bi₃⁺ primary ion gun in static mode. To obtain a flat sample surface (so that better-resolved mass spectra can be achieved), powdery samples were tableted before being fixed at the sample holder using double-sided adhesive tape. The analyzed area of the sample surface was 500 μm × 500 μm. Three spectra from different surfaces were analyzed for each sample. During the analysis, charge neutralization was obtained by using a pulsed low-energy electron flood gun. The number of counts of selected ions from the mass spectra was normalized on the basis of the total ion count for allowing semi-quantitative analysis.

X-ray diffraction (XRD) measurements were performed on a PANalytical X'Pert Pro MPD diffractometer (Malvern PANalytical, Malvern, United Kingdom), using a Cu long-fine focus XRD tube working at 30 mA and 40 kV as an X-ray source. Data were recorded in the 2θ mode with a 0.0167° step (5–90°). Crystalline phases were identified by referring to the ICDD PDF-2 database (version 2004).

X-Ray Photoelectron Spectroscopy (XPS) characterization was performed on a ThermoVG MultilabESCA3000 spectrometer (Thermo Fisher Scientific, Waltham, MA, USA) equipped with an Al K_α anode (hν = 1486.6 eV). The energy shift due to electrostatic charging was subtracted using the contamination sp² carbon C 1s band at 284.6 eV. Contributions with Doniach–Sunjic shape [72] and a S-shaped Shirley type background [73] were used, while the surface atomic ratios and the surface atomic concentrations were obtained using the appropriate experimental sensitivity factors, as determined by Scofield [74].

4.4. Catalytic Tests

The catalysts were tested in the levulinic acid hydrogenation with formic acid as an internal hydrogen source (FALA). The activity tests were performed in a stainless-steel autoclave (Berghof, Eningen, Germany), equipped with a Teflon insert allowing a reaction volume of 45 mL. The FALA

reaction was carried out with 1 g of LA and 0.4 mL of FA aqueous solution at 85% corresponding to a LA/FA equimolar ratio, 0.6 g of catalyst and 30 mL of distilled water. The temperature was maintained at 190 °C for 2 h. After the reaction, the reactor was cooled down to room temperature, the remaining pressure was released, and the mixture was centrifuged to separate the catalyst from the solution. The liquid products were analysed a high-performance liquid chromatograph (Agilent Technologies 1260 Infinity, Perlan Technologies, Santa Clara, CA, USA) equipped with a refractive index detector and Rezex ROA column, using 0.0025 mol·dm⁻³ H₂SO₄ as an eluent. The activity of the catalysts was expressed in terms of LA and FA conversions, and GVL yield, calculated as follows:

$$C_{LA} = \frac{n_{LA_i} - n_{LA_r}}{n_{LA_i}} \cdot 100\% \quad (1)$$

$$C_{FA} = \frac{n_{FA_i} - n_{FA_r}}{n_{FA_i}} \cdot 100\% \quad (2)$$

$$Y_{GVL} = \frac{n_{GVL}}{n_{LA_i}} \cdot 100\% \quad (3)$$

- n_{LA_i} and n_{HMF_r} being the number of moles of LA molecules before and after the reaction respectively, used to calculate the LA conversion (CLA);
- n_{FA_i} and n_{FA_r} being the number of moles of FA molecules before and after the reaction respectively, used to calculate the FA conversion (CFA);
- and n_{GVL} being the number of moles of GVL molecules produced and used to calculate the GVL yield (Y_{GVL}).

The catalysts were tested in the hydrogenation of 5-(hydroxymethyl)furfural. The tests were performed in a 60 mL stainless-steel autoclave (Premex, Bolton, UK) with 1 g of 5-HMF, 0.15 g of catalyst and 30 mL of 1,4 dioxane as a solvent. After purging 2 times with H₂, the reactor was pressurized with H₂ to 30 bar and heated at 220 °C for 4 h under stirring. After the reaction, the reactor was cooled down to room temperature, the remaining pressure was released, and the mixture was centrifuged to separate the catalyst from the solution. The products were subsequently injected into a GC-FID (Agilent 7890A, CP-Wax 52 CB capillary column, Santa Clara, CA, USA). The activity of the catalysts was expressed in terms of HMF conversion and of reaction yields to given products, calculated as follows:

$$\text{Conversion} = \frac{n_{HMF_i} - n_{HMF_r}}{n_{HMF_i}} \cdot 100\% \quad (4)$$

$$\text{Yield} = \frac{n_{\text{prod}}}{n_{HMF_i}} \cdot 100\% \quad (5)$$

- n_{HMF_i} and n_{HMF_r} being the number of moles of HMF molecules before and after the reaction, respectively, and n_{prod} being the number of moles of a given product in the reaction mixture.

All catalytic tests in both LA and HMF hydrogenation reactions were duplicated, and the obtained results remained within a ±2% accuracy range. The average data are presented in Tables 3 and 4.

5. Conclusions

We showed that the Ni:Pd metal ratio strongly influences the activity, and more globally, the catalytic behavior of the Ni-Pd/γ-Al₂O₃ catalysts in both LA hydrogenation into GVL using FA as an internal hydrogen source and HMF hydrodeoxygenation. Interestingly, the influence of the Ni:Pd ratio was strongly dependent on the hydrogenation reaction. Monometallic Ni catalyst shows low activity in both processes, due to a low number of active metallic sites, as a result of strong nickel/alumina interactions, that may favor the formation of the detrimental aluminate spinel interfacial phase. The Pd-modified Ni-rich system shows boosted activity due to a higher number of Ni active

sites, while Pd is proposed to be a spectator species for the reaction. By contrast, the much higher Pd active site availability in the Ni-modified Pd-rich catalyst, in comparison to its monometallic Pd counterpart associated with maintaining a very high surface acidity, was proposed to push the HMF hydro-deoxygenation forward and consequently to achieve a higher BHMTHF selectivity. Beside the role of metals, residual chlorine was suggested to positively influence the metals/support interactions and consequently to alter the catalyst properties.

By testing the catalysts in two hydrogenation reactions that require different site-specific properties, we showed also the broader aspect of this work which can be easily extended for other high impact hydrogenation processes of high industrial relevance, for which activity and even more selectivity aspects remain crucial.

Supplementary Materials: The following are available online at <http://www.mdpi.com/2073-4344/10/9/1026/s1>, Figure S1: XRD patterns of mono- and bi-metallic catalysts, Figure S2: TPR profiles of the mono- and bi-metallic catalysts after the reduction step, Figure S3: Wide scan survey XPS spectra of the mono and bimetallic catalysts. Figure S4: FTIR spectra of CO adsorbed on the surface of (a) the monometallic and (b) the bimetallic catalysts recorded after CO evacuation.

Author Contributions: Conceptualization, A.M.R.; supervision, A.M.R.; funding acquisition, A.M.R.; project administration, A.M.R.; writing—original draft preparation, E.S., N.K. and A.M.R.; methodology, A.M.R.; investigations, E.S., M.J., I.K. and N.K. All authors have read and agreed to the published version of the manuscript.

Funding: The authors gratefully acknowledge that this work was financially supported by a grant SONATA BIS from the National Center of Science (NCN) in Krakow (Poland) (2016/22/E/ST4/00550).

Acknowledgments: V. Papaefthimiou (ICPEES) is thanked for performing XPS analysis.

Conflicts of Interest: The authors declare no conflict of interest.

References

1. Ruppert, A.M.; Weinberg, K.; Palkovits, R. Hydrogenolysis Goes Bio: From Carbohydrates and Sugar Alcohols to Platform Chemicals. *Angew. Chem. Int. Ed.* **2012**, *51*, 2564–2601. [[CrossRef](#)]
2. Alonso, D.M.; Bond, J.Q.; Dumesic, J.A. Catalytic conversion of biomass to biofuels. *Green Chem.* **2010**, *12*, 1493–1513. [[CrossRef](#)]
3. Xu, C.; Ouyang, W.; Muñoz-Batista, M.J.; Fernández-García, M.; Luque, R. Highly active catalytic Ru/TiO₂ nanomaterials for continuous flow production of γ -valerolactone. *ChemSusChem* **2018**, *15*, 2604–2611. [[CrossRef](#)]
4. Zhang, R.; Ma, Y.; You, F.; Peng, T.; He, Z.; Li, K. Exploring to direct the reaction pathway for hydrogenation of levulinic acid into γ -valerolactone for future Clean-Energy Vehicles over a magnetic Cu-Ni catalyst. *Int. J. Hydrog. Energy.* **2017**, *40*, 25185–25194. [[CrossRef](#)]
5. Chen, S.; Wojcieszak, R.; Dumeignil, F.; Marceau, E.; Royer, S. How Catalysts and Experimental Conditions Determine the Selective Hydroconversion of Furfural and 5-Hydroxymethylfurfural. *Chem. Rev.* **2018**, *118*, 11023–11117. [[CrossRef](#)]
6. Kong, X.; Zhu, Y.; Zheng, H.; Dong, F.; Zhu, Y.; Li, Y. Switchable synthesis of 2,5-dimethylfuran and 2,5-dihydroxymethyltetrahydrofuran from 5-hydroxymethylfurfural over Raney Ni catalyst. *RSC Adv.* **2014**, *4*, 60467–60472. [[CrossRef](#)]
7. Lima, S.; Chadwick, D.; Hellgardt, K. Towards sustainable hydrogenation of 5-(hydroxymethyl)furfural: A two-stage continuous process in aqueous media over RANEY[®] catalysts. *RSC Adv.* **2017**, *7*, 31401–31407. [[CrossRef](#)]
8. Delidovich, I.; Hausoul, P.J.C.; Deng, L.; Pfutzentreuter, R.; Rose, M.; Palkovits, R. Alternative Monomers Based on Lignocellulose and Their Use for Polymer Production. *Chem. Rev.* **2016**, *116*, 1540–1599. [[CrossRef](#)]
9. Buntara, T.; Noel, S.; Phua, P.H.; Melian-Cabrera, I.; de Vries, J.G.; Heeres, H.J. Caprolactam from Renewable Resources: Catalytic Conversion of 5-Hydroxymethylfurfural into Caprolactone. *Angew. Chem. Int. Ed.* **2011**, *50*, 7083–7087. [[CrossRef](#)]
10. Cai, H.; Li, C.; Wang, A.; Zhang, T. Biomass into chemicals: One-pot production of furan-based diols from carbohydrates via tandem reactions. *Catal. Today* **2014**, *234*, 59–65. [[CrossRef](#)]

11. Sudhakar, M.; Kumar, V.V.; Naresh, G.; Kantam, M.L.; Bhargava, S.K.; Venugopal, A. Vapor phase hydrogenation of aqueous levulinic acid over hydroxyapatite supported metal (M = Pd,Pt,Ru,Cu,Ni) catalysts. *Appl. Catal. B Environ.* **2016**, *180*, 113–120. [[CrossRef](#)]
12. Dutta, S.; Yu, I.K.M.; Tsang, D.C.W.; Ng, Y.H.; Ok, Y.S.; Sherwood, J.; Clark, J.H. Green synthesis of gamma-valerolactone (GVL) through hydrogenation of biomass-derived levulinic acid using non-noble metal catalysts: A critical review. *Chem. Eng. J.* **2019**, *372*, 992–1006. [[CrossRef](#)]
13. Zhang, Y.; Wang, B.; Qin, L.; Li, Q.; Fan, Y. Non-noble bimetallic alloy in the high selective electrochemical synthesis of biofuel 2, 5-dimethyl-furan from 5-hydroxymethylfurfural. *Green Chem.* **2019**, *21*, 1108–1113. [[CrossRef](#)]
14. Duarte, D.P.; Martinez, R.; Hoyos, L.I. Hydrodeoxygenation of 5-hydroxymethylfurfural over alumina-supported catalysts in aqueous medium. *Ind. Eng. Chem. Res.* **2016**, *55*, 54–63. [[CrossRef](#)]
15. Kong, X.; Zheng, R.; Zhu, Y.; Ding, G.; Zhu, Y.; Li, Y. Rational Design of Ni-based Catalysts derived from Hydrotalcite for Selective Hydrogenation of 5-Hydroxymethylfurfural. *Green Chem.* **2015**, *17*, 2504–2514. [[CrossRef](#)]
16. Ruppert, A.M.; Jędrzejczyk, M.; Potrzebowska, N.; Kaźmierczak, K.; Brzezińska, M.; Sneka-Płatek, O.; Sautet, P.; Keller, N.; Michel, C.; Grams, J. Supported gold-nickel nano-alloy as highly efficient catalyst in levulinic acid hydrogenation with formic acid as an internal hydrogen source. *Catal. Sci. Technol.* **2018**, *8*, 4318–4331. [[CrossRef](#)]
17. Nakagawa, Y.; Tomishige, K. Total hydrogenation of furan derivatives over silica-supported Ni–Pd alloy catalyst. *Catal. Comm.* **2010**, *12*, 154–156. [[CrossRef](#)]
18. Soszka, E.; Reijneveld, H.M.; Jędrzejczyk, M.; Rzeźnicka, I.; Grams, J.; Ruppert, A.M. Chlorine influence on palladium doped nickel catalysts in levulinic acid hydrogenation with formic acid as hydrogen source. *ACS Sustain. Chem. Eng.* **2018**, *6*, 14607–14613. [[CrossRef](#)]
19. Mihet, M.; Lazar, M.D. Effect of Pd and Rh promotion on Ni/Al₂O₃ for NO reduction by hydrogen for stationary applications. *Chem. Eng. J.* **2014**, *251*, 310–318. [[CrossRef](#)]
20. Mihet, M.; Lazar, M.D. Methanation of CO₂ on Ni/γ-Al₂O₃: Influence of Pt, Pd or Rh promotion. *Catal. Today* **2018**, *306*, 294–299. [[CrossRef](#)]
21. Dias, J.A.C.; Assaf, J.M. Autothermal reforming of methane over Ni/γ-Al₂O₃ promoted with Pd The effect of the Pd source in activity, temperature profile of reactor and in ignition. *Appl. Catal. A-Gen.* **2008**, *334*, 243–250. [[CrossRef](#)]
22. Bayat, N.; Rezaei, M.; Meshkani, F. Hydrogen and carbon nanofibers synthesis by methane decomposition over Ni-Pd/Al₂O₃ catalyst. *Int. J. Hydrog. Energy.* **2016**, *41*, 5494–5503. [[CrossRef](#)]
23. Zhang, J.; Wang, Y.; Wu, D. Hydrogen Production from Partial Oxidation and Steam Reforming of N-octane Over Alumina-supported Ni and Ni-Pd Catalysts. *Can. J. Chem. Eng.* **2003**, *81*, 307–311. [[CrossRef](#)]
24. Zhang, J.; Wang, Y.; Ma, R.; Wu, D. Investigation of Alumina-Supported Ni and Ni-Pd Catalysts by Partial Oxidation and Steam Reforming of n-Octane. *Korean J. Chem. Eng.* **2003**, *20*, 288–292. [[CrossRef](#)]
25. Alamillo, R.; Tucker, M.; Chia, M.; Pagan-Torres, Y.; Dumesic, J.A. The selective hydrogenation of biomass-derived 5-hydroxymethylfurfural using heterogeneous catalysts. *Green Chem.* **2012**, *14*, 1413–1419. [[CrossRef](#)]
26. Davda, R.R.; Shabaker, J.W.; Huber, G.W.; Cortright, R.D.; Dumesic, J.A. Aqueous-phase reforming of ethylene glycol on silica-supported metal catalysts. *Appl. Catal. B Environ.* **2003**, *43*, 13–26. [[CrossRef](#)]
27. Chen, H.; Li, T.; Jiang, F.; Wang, Z. Enhanced catalytic reduction of N-nitrosodimethylamine over bimetallic Pd-Ni catalysts. *J. Mol. Catal. A Chem.* **2016**, *421*, 167–177. [[CrossRef](#)]
28. Hilli, Y.; Kinnunen, N.M.; Suvanto, M.; Savimäki, A.; Kallinen, K.; Pakkanen, T.A. Preparation and characterization of Pd–Ni bimetallic catalysts for CO and C₃H₆ oxidation under stoichiometric conditions. *Appl. Catal. A Gen.* **2015**, *497*, 85–95. [[CrossRef](#)]
29. Sales, E.A.; Jove, J.; Mendes, M.J.; Bozon-Varduraz, F. Palladium, Palladium–Tin, and Palladium–Silver Catalysts in the Selective Hydrogenation of Hexadienes: TPR, Mössbauer, and Infrared Studies of Adsorbed CO. *J. Catal.* **2000**, *195*, 88–95. [[CrossRef](#)]
30. Esteves, L.M.; Brijaldo, M.H.; Passos, F.B. Decomposition of acetic acid for hydrogen production over Pd/Al₂O₃ and Pd/TiO₂: Influence of metal precursor. *J. Mol. Catal. A Chem.* **2016**, *422*, 275–288. [[CrossRef](#)]
31. Luo, M.; Hou, Z.; Yuan, X.; Zheng, X. Characterization study of CeO₂ supported Pd catalyst for low-temperature carbon monoxide oxidation. *Catal. Lett.* **1998**, *50*, 205–209. [[CrossRef](#)]

32. Mukainakano, Y.; Li, B.; Kado, S.; Miyazawa, T.; Okumura, K.; Miyao, T.; Naito, S.; Kunimori, K.; Tomishige, K. Surface modification of Ni catalysts with trace Pd and Rh for oxidative steam reforming of methane. *App. Catal. A Gen.* **2007**, *318*, 252–264. [[CrossRef](#)]
33. Babu, N.S.; Lingaiah, N.; Sai Prasad, P.S. Characterization and reactivity of Al₂O₃ supported Pd-Ni bimetallic catalysts for hydrodechlorination of chlorobenzene. *Appl. Catal. B* **2012**, *111–112*, 309–316. [[CrossRef](#)]
34. Nag, N.K. A Study on the Formation of Palladium Hydride in a Carbon-Supported Palladium Catalyst. *J. Phys. Chem. B* **2001**, *105*, 5945–5949. [[CrossRef](#)]
35. Babu, N.S.; Lingaiah, N.; Gopinath, R.; Reddy, P.S.S. Prasad, Characterization and Reactivity of Alumina-Supported Pd Catalysts for the Room-Temperature Hydrodechlorination of Chlorobenzene. *J. Phys. Chem. C* **2007**, *111*, 6447–6453. [[CrossRef](#)]
36. Bykova, M.V.; Ermakov, D.Y.; Kaichev, V.V.; Bulavchenko, O.A.; Saraev, A.A.; Lebedev, M.Y.; Yakovlev, V.A. Ni-based sol-gel catalysts as promising systems for crude bio-oil upgrading: Guaiacol hydrodeoxygenation study. *Appl. Catal. A* **2012**, *113*, 296–307. [[CrossRef](#)]
37. Dube, C.E.; Workie, B.; Kounaves, S.P.; Rabbat, A.; Aksu, M.L., Jr.; Davies, G.J. Electrodeposition of Metal Alloy and Mixed Oxide Films Using a Single-Precursor Tetranuclear Copper-Nickel Complex. *Electrochem. Soc.* **1995**, *142*, 3357–3365.
38. Li, C.P.; Proctor, A.; Hercules, D.M. Curve Fitting Analysis of ESCA Ni 2p Spectra of Nickel-Oxygen Compounds and Ni/Al₂O₃ Catalysts. *Appl. Spectrosc.* **1984**, *38*, 880–886. [[CrossRef](#)]
39. Betti, C.; Carrara, N.; Badano, J.; Lederhos, C.; Vera, C.; Quiroga, M. MORE ACTIVE AND SULFUR RESISTANT BIMETALLIC Pd-Ni CATALYSTS. *Quim. Nova* **2018**, *41*, 151–156. [[CrossRef](#)]
40. Moulder, J.F.; Stickle, W.F.; Sobol, P.E.; Bomben, K.D. *Handbook of X-ray Photoelectron Spectroscopy*; Chastain, J., Ed.; Perkin-Elmer Corporation: Norwalk, CT, USA, 1992.
41. Ruppert, A.M.; Jędrzejczyk, M.; Sneka-Platek, O.; Keller, N.; Dumon, A.S.; Michel, C.; Sautet, P.; Grams, J. Ru catalysts for levulinic acid hydrogenation with formic acid as a hydrogen source. *Green Chem.* **2016**, *18*, 2014–2028. [[CrossRef](#)]
42. Schmal, M.; Aranda, D.A.G.; Noronha, F.B.; Guimaraes, A.L.; Monteiro, R.S. Oxidation and reduction effects of propane-oxygen on Pd-chlorine/alumina catalysts. *Catal. Lett.* **2000**, *64*, 163–169. [[CrossRef](#)]
43. Mazzieri, V.; Coloma-Pascual, F.; Arcoya, A.; L'Argentiere, P.C.; Figoli, N.S. XPS, FTIR and TPR characterization of Ru/Al₂O₃ catalysts. *Appl. Surf. Sci.* **2003**, *210*, 222–230. [[CrossRef](#)]
44. Zhao, Y.; Liang, W.; Li, Y.; Lefferts, L. Effect of chlorine on performance of Pd catalysts prepared via colloidal immobilization. *Catal. Today* **2017**, *297*, 308–315. [[CrossRef](#)]
45. Zhao, H.; Jin, L.; Zhou, Y.; Bandar, A.; Fan, Z.; Govorov, A.O.; Mi, Z.; Sun, S.; Rosei, F.; Vomiero, A. Green synthesis of near infrared core/shell quantum dots for photocatalytic hydrogen production. *Nanotechnology* **2016**, *27*, 495405. [[CrossRef](#)]
46. Dogu, D.; Meyer, K.E.; Fuller, A.; Gunduz, S.; Deka, D.J.; Kramer, N.; Co, A.C.; Ozkan, U.S. Effect of Lanthanum and Chlorine Doping on Strontium Titanates for the Electrocatalytically-Assisted Oxidative Dehydrogenation of Ethane. *Appl. Catal. B Environ.* **2018**, *227*, 90–101. [[CrossRef](#)]
47. Mihaylov, M.; Hadjiivanov, K.; Knozinger, H. Formation of Ni(CO)₄ during the interaction between CO and silica-supported nickel catalyst: An FTIR spectroscopic study. *Catal. Lett.* **2001**, *76*, 59–63. [[CrossRef](#)]
48. Liberatori, J.W.C.; Ribeiro, R.U.; Zanchet, D.; Noronha, F.B.; Bueno, J.M.C. Steam reforming of ethanol on supported nickel catalysts. *Appl. Catal. A Gen.* **2007**, *327*, 197–204. [[CrossRef](#)]
49. Dulaurent, O.; Chandes, K.; Bouly, C.; Bianchi, D. Heat of Adsorption of Carbon Monoxide on a Pd/Al₂O₃ Solid Using in Situ Infrared Spectroscopy at High Temperatures. *J. Catal.* **1999**, *188*, 237–251. [[CrossRef](#)]
50. Tiznado, H.; Fuentes, S.; Zaera, F. Infrared Study of CO Adsorbed on Pd/Al₂O₃-ZrO₂. Effect of Zirconia Added by Impregnation. *Langmuir* **2004**, *20*, 10490–10497. [[CrossRef](#)]
51. Tessie, D.; Rakai, A.; Bozon-Verduraz, F. Spectroscopic Study of the Interaction of Carbon Monoxide with Cationic and Metallic Palladium in Palladium-Alumina Catalysts. *J. Chem. Soc. Faraday Trans.* **1992**, *88*, 741–749. [[CrossRef](#)]
52. Blyholder, G. Molecular Orbital View of Chemisorbed Carbon Monoxide. *Am. J. Phys. Chem.* **1964**, *10*, 2772–2777. [[CrossRef](#)]
53. Skotak, M.; Karpinski, Z.; Juszczak, W.; Pielaszeka, J.; Kepinski, L.; Kazachkin, D.V.; Kovalchuk, V.I.; d'Itri, J.L. Characterization and catalytic activity of differently pretreated Pd/Al₂O₃ catalysts: The role of acid sites and of palladium-alumina interactions. *J. Catal.* **2004**, *227*, 11–25. [[CrossRef](#)]

54. Lear, T.; Marshall, R.; Lopez-Sanchez, J.A.; Jackson, S.D.; Klapotke, T.M.; Baumer, M.; Rupprechter, G.; Freund, H.; Lennon, D. The application of infrared spectroscopy to probe the surface morphology of alumina-supported palladium catalysts. *J. Chem. Phys.* **2005**, *123*, 174706. [[CrossRef](#)]
55. Garland, C.W.; Lord, R.C.; Troiano, P.F. An Infrared Study of High-Area Metal Films Evaporated in Carbon Monoxide. *Am. J. Phys. Chem.* **1965**, *4*, 1188–1195. [[CrossRef](#)]
56. Karthikeyan, D.; Lingappan, N.; Sivasankar, B.; Jabarithnam, N.J. Activity and selectivity for hydroisomerisation of n-decane over Ni impregnated Pd/H-mordenite catalysts. *Appl. Catal. A Gen.* **2008**, *345*, 18–27. [[CrossRef](#)]
57. Prinetto, F.; Manzoli, M.; Ghiotti, G.; Ortis, M.M.; Tichit, D.; Coq, B. Pd/Mg(Al)O catalysts obtained from hydrotalcites: investigation of acid–base properties and nature of Pd phases. *J. Catal.* **2004**, *222*, 238–249. [[CrossRef](#)]
58. Early, K.; Kovalcuk, V.I.; Lonyi, F.; Deshmukh, S.; d'Itri, J.L. Hydrodechlorination of 1,1-Dichlorotetrafluoroethane and Dichlorodifluoromethane Catalyzed by Pd on Fluorinated Aluminas: The Role of Support Material. *J. Catal.* **1999**, *182*, 219–227. [[CrossRef](#)]
59. Digne, M.; Raybaud, P.; Sautet, P.; Guillaume, D.; Toulhoat, H. Atomic Scale Insights on Chlorinated γ -Alumina Surfaces. *J. Am. Chem. Soc.* **2008**, *130*, 11030–11039. [[CrossRef](#)]
60. Bozon-Verduraz, F.; Omar, A.; Escard, J.; Pontvianne, B. Chemical State and Reactivity of Supported Palladium. *J. Catal.* **1978**, *53*, 126–134. [[CrossRef](#)]
61. Mahata, N.; Raghavan, K.V.; Vishwanathan, V.; Park, C.; Keane, M.A. Phenol hydrogenation over palladium supported on magnesia: Relationship between catalyst structure and performance. *Phys. Chem.* **2001**, *3*, 2712–2719. [[CrossRef](#)]
62. Mahata, N.; Vishwanathan, V. Influence of Palladium Precursors on Structural Properties and Phenol Hydrogenation Characteristics of Supported Palladium Catalysts. *J. Catal.* **2000**, *196*, 262–270. [[CrossRef](#)]
63. Seoane, X.L.; L'Argentiere, P.C.; Figoli, N.S.; Arcoya, A. On the deactivation of supported palladium hydrogenation catalysts by thiophene poisoning. *Catal. Lett.* **1992**, *16*, 137–148. [[CrossRef](#)]
64. Al-Shammeri, K.K.; Saleh, J.M. Adsorption and Decomposition of Ammonia on Metal Films of Nickel, Palladium, Tungsten, and Aluminum. *J. Phys. Chem.* **1986**, *90*, 2906–2910. [[CrossRef](#)]
65. Perret, N.; Grigoropoulos, A.; Zanella, M.; Manning, T.D.; Claridge, J.B.; Rosseinsky, M.J. Catalytic Response and Stability of Nickel/Alumina for the Hydrogenation of 5-Hydroxymethylfurfural in Water. *ChemSusChem* **2016**, *9*, 521–531. [[CrossRef](#)] [[PubMed](#)]
66. Chidambaram, M.; Bell, A.T. A two-step approach for the catalytic conversion of glucose to 2,5-dimethylfuran in ionic liquids. *Green Chem.* **2010**, *12*, 1253–1262. [[CrossRef](#)]
67. Mitra, J.; Zhou, X.; Rauchfuss, T. Pd/C-catalyzed reactions of HMF: Decarbonylation, hydrogenation, and hydrogenolysis. *Green Chem.* **2015**, *17*, 307–313. [[CrossRef](#)]
68. Cheng, C.K.; Foo, S.Y.; Adesina, A.A. Steam reforming of glycerol over Ni/Al₂O₃ catalyst. *Catal. Today* **2011**, *178*, 25–33. [[CrossRef](#)]
69. Kumar, V.V.; Naresh, G.; Sudhakar, M.; Anjaneyulu, C.; Bhargava, S.K.; Tardio, J.; Reddy, V.K.; Padmasric, A.H.; Venugopal, A. An investigation on the influence of support type for Ni catalysed vapour phase hydrogenation of aqueous levulinic acid to γ -valerolactone. *RSC Adv.* **2016**, *6*, 9872–9879. [[CrossRef](#)]
70. Nikolić, V.D.; Kamberović, Ž.J.; Korać, M.S.; Anđić, Z.M.; Mihajlović, A.M.; Uljarević, J.B. Nickel-based catalysts: Dependence of properties on nickel loading and modification with palladium. *Chem. Ind.* **2016**, *70*, 137–142. [[CrossRef](#)]
71. Kocemba, I. Apparatus for investigation of catalysts by temperature programmed methods. *Przem. Chem.* **2003**, *3*, 142–145.
72. Doniach, S.; Sunjic, M. Many-electron singularity in X-ray photoemission and X-ray line spectra from metals. *J. Phys. C Solid State Phys.* **1970**, *3*, 2. [[CrossRef](#)]
73. Shirley, D.A. High-Resolution X-Ray Photoemission Spectrum of the Valence Bands of Gold. *Phys. Rev. B* **1972**, *5*, 4709. [[CrossRef](#)]
74. Scofield, J.H. Hartree-Slater subshell photoionization cross-sections at 1254 and 1487 eV. *J. Electron Spectrosc. Relat. Phenom.* **1976**, *8*, 129–137. [[CrossRef](#)]

